Journal of Medicinal Chemistry

Article

pubs.acs.org/jmc

Influence of the Bifunctional Chelator on the Pharmacokinetic Properties of $^{99m}Tc(CO)_3$-Labeled Cyclic α-Melanocyte Stimulating Hormone Analog

Maurício Morais,[†] Bruno L. Oliveira,[†] João D. G. Correia,[†] Maria Cristina Oliveira,[†] Maria Angeles Jiménez,[‡] Isabel Santos,*[,†] and Paula D. Raposinho[†]

[†]Unidade de Ciências Químicas e Radiofarmacêuticas, IST/ITN, Instituto Superior Técnico, Universidade Técnica de Lisboa, Estrada Nacional 10, 2686-953, Sacavém, Portugal

[‡]Instituto de Química Física Rocasolano, Consejo Superior de Investigaciones Científicas (CSIC), Serrano 119, 28006 Madrid, Spain

Supporting Information

ABSTRACT: Aiming at the design of specific melanocortin-1 receptor (MC1R) targeted imaging probes, we report on the effect of different azolyl-ring substitution patterns (carboxylate at the 4-position and/or methyl groups at the 3,5 positions) of pyrazolyl-diamine bifunctional chelators (Pz^2–Pz^4) on the pharmacokinetic profile of the $^{99m}Tc(CO)_3$-labeled lactam bridge-cyclized α-melanocyte stimulating hormone derivative, βAlaNleCycMSH$_{hex}$. Three pyrazolyl-diamine-containing chelators were conjugated to βAlaNleCycMSH$_{hex}$, with the resulting peptide conjugates displaying subnanomolar MC1R binding affinity. Biodistribution studies in B16F1 melanoma-bearing mice show that all radiopeptides present a good melanoma uptake. The introduction of a carboxylate group in the azolyl-ring leads to a remarkable reduction of the kidney (>89%) and liver (>91%) accumulation for $^{99m}Tc(CO)_3$-Pz^3-βAlaNleCycMSH$_{hex}$ and $^{99m}Tc(CO)_3$-Pz^4-βAlaNleCycMSH$_{hex}$ when compared to the radiopeptide $^{99m}Tc(CO)_3$-Pz^1-βAlaNleCycMSH$_{hex}$, where that group is absent. The good tumor uptake and favorable tumor-to-nontarget-organs ratios of $^{99m}Tc(CO)_3$-Pz^3-βAlaNleCycMSH$_{hex}$ and $^{99m}Tc(CO)_3$-Pz^4-βAlaNleCycMSH$_{hex}$ highlights the potential of both compounds as melanoma imaging agents.

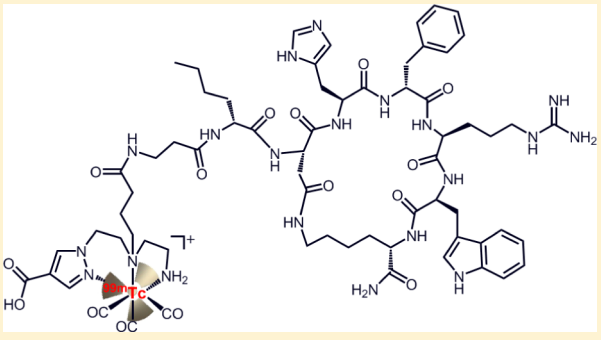

INTRODUCTION

Various linear and cyclic radiolabeled α-melanocyte-stimulating hormone (α-MSH: Ac-Ser[1]-Tyr[2]-Ser[3]-Met[4]-Glu[5]-His[6]-Phe[7]-Arg[8]-Trp[9]-Gly[10]-Lys[11]-Pro[12]-Val[13]-NH_2) analogues have been explored as radiopharmaceuticals for melanoma imaging and therapy by specifically probing melanocortin-1 receptor (MC1R), a molecular target that is overexpressed on both human and mouse melanoma cells.[1−3] The radiopeptides with the most interesting melanoma-targeting properties are based on cyclic derivatives that display high metabolic stability and enhanced receptor-binding affinity. Among them, ^{99m}Tc and ^{111}In-labeled metal-cyclized and lactam bridge-cyclized peptides displayed the highest melanoma uptake and lowest renal accumulation in B16F1 melanoma-bearing mice and became the most promising tools to be further explored as potential melanoma imaging probes.[1,4] Over the past years, Quinn's and Miao's groups have designed a family of ^{111}In-labeled metal- and lactam bridge-cyclized 1,4,7,10-tetraazacyclododecane-1,4,7,10-tetraacetic acid (DOTA)-conjugated α-MSH analogues for melanoma imaging and concluded that the reduction of the peptide ring size increases the melanoma uptake, decreasing kidney accumulation.[5−7] Among them, the metal-cyclized ^{111}In-DOTA-Re(Arg[11])CCMSH and the lactam bridge-cyclized ^{111}In-DOTA-NleCycMSH$_{hex}$ presented high melanoma uptake and comparable tumor-to-kidney ratios in B16F1 melanoma-bearing mice (Figure 1).[6,7] More recently, it has also been reported that the introduction of a Gly−Gly linker in ^{111}In-DOTA-NleCycMSH$_{hex}$ leads to a radiopeptide (^{111}In-DOTA-GlyGlyNleCycMSH$_{hex}$) with similar melanoma uptake and improved tumor-to-kidney ratio (Figure 1).[8]

The effect of ring size reduction was also considered on the design of ^{67}Ga-labeled-lactam bridge-cyclized α-MSH derivatives for melanoma imaging in B16F1 tumor-bearing mice.[9,10] The peptide GlyGlyNleCycMSH$_{hex}$ (6-amino acid peptide ring) was conjugated to triazacyclononane-1,4,7-triacetic acid (NOTA) and DOTA and labeled with ^{67}Ga. The radiopeptide ^{67}Ga-NOTA-GlyGlyNle-CycMSH$_{hex}$ displayed the highest melanoma uptake and tumor-to-kidney ratios as compared to all described ^{111}In- and ^{67}Ga-labeled cyclic α-MSH derivatives.[10]

Considering our interest in the design of specific $^{99m}Tc(CO)_3$-labeled peptides for MC1R targeting, we have recently reported the cyclic radiopeptide $^{99m}Tc(CO)_3$-Pz^1-βAlaNle-

Received: November 7, 2012
Published: February 17, 2013

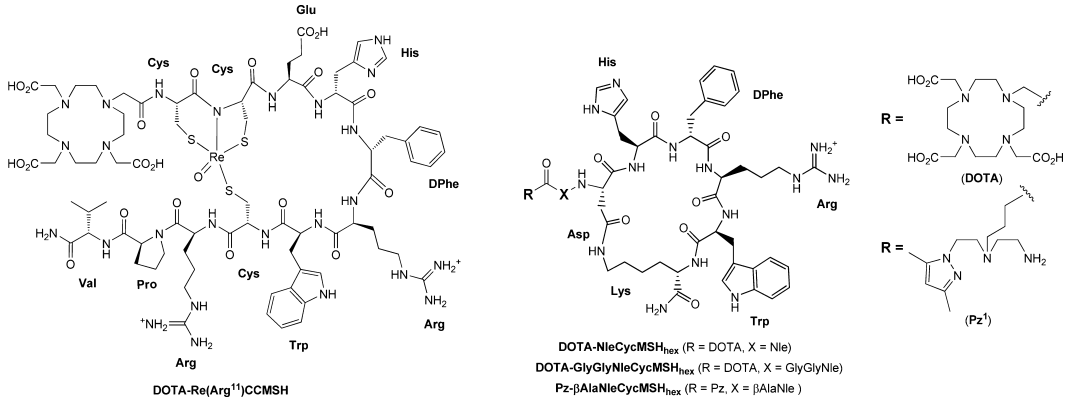

Figure 1. Metal-cyclized and lactam bridge-cyclized α-MSH derivatives: structures of DOTA-Re(Arg^{11})CCMSH, DOTA-NleCycMSH$_{hex}$, DOTA-GlyGlyNleCycMSH$_{hex}$, and Pz^1-βAlaNleCycMSH$_{hex}$.

CycMSH$_{hex}$ (Figure 1).[11,12] The biological evaluation of this radiopeptide in B16F1 melanoma-bearing mice has shown a significant tumor uptake (11.3 ± 1.8% IA/g) at 4 h post injection (pi), although presenting slow overall excretion rate (37.4 ± 2.4 percentage injected activity per gram, % IA/g) and high accumulation in excretory organs (32.1 ± 1.6% and 22.9 ± 1.2% IA/g for kidney and liver, respectively). This high melanoma uptake, which compares well with the values found for ^{111}In-labeled DOTA-NleCycMSH$_{hex}$ (17.0 ± 2.5% IA/g, at 4h pi) and DOTA-GlyGlyNleCycMSH$_{hex}$ (18.6 ± 3.5% IA/g, at 4h pi) in the same animal model, prompted the design of new ^{99m}Tc(I)-labeled βAlaNleCycMSH$_{hex}$ derivatives with improved pharmacokinetic profile.[4]

It is generally accepted that the overall biological profile of radiolabeled peptides is determined by receptor-specific binding but also by "nonspecific" interactions, which most likely rely on the overall physicochemical features of the radiopeptides (e.g., molecular weight, overall charge, and lipophilicity).[13,14] To modulate such physicochemical properties, several approaches have been explored, namely the nature of the chelator,[15] the net charge of the chelator–peptide conjugate,[15,16] the presence of carbohydrate moieties,[17] and the reduction of the peptide size.[7,18] Having this in mind, we decided to investigate the overall biological profile of ^{99m}Tc(CO)$_3$-labeled βAlaNleCycMSH$_{hex}$ as a function of structural modifications in the ring substitution pattern of the pyrazolyl-diamine chelators. Such data would provide a better insight into the structural factors that modulate/influence melanoma uptake, overall excretion rate, and tumor-to-nontarget organs ratios in melanoma bearing mice.

RESULTS

Synthesis and Characterization of the Pyrazolyl-Diamine Derivatives. Profiting from the versatility of the asymmetric pyrazolyl-diamine-containing bifunctional chelator (BFC) demonstrated in the labeling of a wide range of biomolecules,[19−22] we have selected the pyrazolyl derivatives Pz^2–Pz^4 with a *N,N,N* donor atom set for stabilization of the organometallic core *fac*-[M(CO)$_3$]$^+$ (M = Re, ^{99m}Tc) and bearing a propyl linker for peptide conjugation (Figure 2).

As depicted in Scheme 1, the *tert*-butyloxycarbonyl (Boc)-protected chelators Pz^2(Boc), Pz^3(Boc), and *t*-BuPz^4(Boc) were prepared by alkylation of the central secondary amine of precursors **1**, **2**, and **3**, respectively, with ethyl 4-bromobutanoate, and basic hydrolysis of the corresponding intermediate

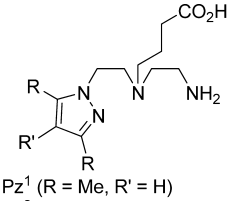

Figure 2. Tridentate asymmetric pyrazolyl-containing bifunctional chelators Pz^1–Pz^4.

compounds **4**, **5**, and **6**, following synthetic procedures previously described by our group.[23,26]

All compounds have been characterized by the usual analytical techniques in chemistry, including reverse-phase high performance liquid chromatography (RP-HPLC), nuclear magnetic resonance (NMR), and electrospray ionization–mass spectrometry (ESI-MS).

Synthesis and Characterization of the Peptide Conjugates. The chelators Pz^2(Boc), Pz^3(Boc), and *t*-BuPz^4(Boc) were conjugated to βAlaNleCycMSH$_{hex}$ via 2-(7-aza-1*H*-benzotriazole-1-yl)-1,1,3,3-tetramethyluronium hexafluorophosphate (HATU) activation in the presence of diisopropylethylamine (DIPEA), yielding intermediate conjugates, which, upon treatment with trifluoracetic acid (TFA), gave the final conjugates Pz^2-βAlaNleCycMSH$_{hex}$, Pz^3-βAlaNleCycMSH$_{hex}$, and Pz^4-βAlaNleCycMSH$_{hex}$, respectively (Scheme 2).

The conjugates were purified by semipreparative RP-HPLC and characterized by ESI-MS (Table 1).

Owing to the existence of two free carboxylate groups in Pz^3(Boc), one at the pyrazole ring and the other at the aliphatic arm, there are two likely conjugation positions for the peptide. To clarify this point, solution NMR studies for Pz^3 and Pz^3-βAlaNleCycMSH$_{hex}$ have been performed. After assigning the resonances in the spectra of Pz^3 and Pz^3-βAlaNleCycMSH$_{hex}$, we found that the chemical shifts of the carbon atoms of the pyrazolyl ring in Pz^3 and Pz^3-βAlaNleCycMSH$_{hex}$ were almost identical (^{13}C: $|\Delta\delta^{free\text{-}bound}| \leq 0.5$ ppm; Supporting Information Table ST2), while a significant difference was found for the methylene carbons of the aliphatic arm (1.1 and 1.7 ppm for methylene carbons C^i and C^j, respectively; Supporting Information Table ST2), indicating that the conjugation occurs by the carboxylate group at the aliphatic arm. Stronger and

dx.doi.org/10.1021/jm301647t | J. Med. Chem. 2013, 56, 1961−1973

Scheme 1. Synthesis of the Bifunctional Chelators Pz^2(Boc), Pz^3(Boc), and *t*-BuPz^4(Boc)[a]

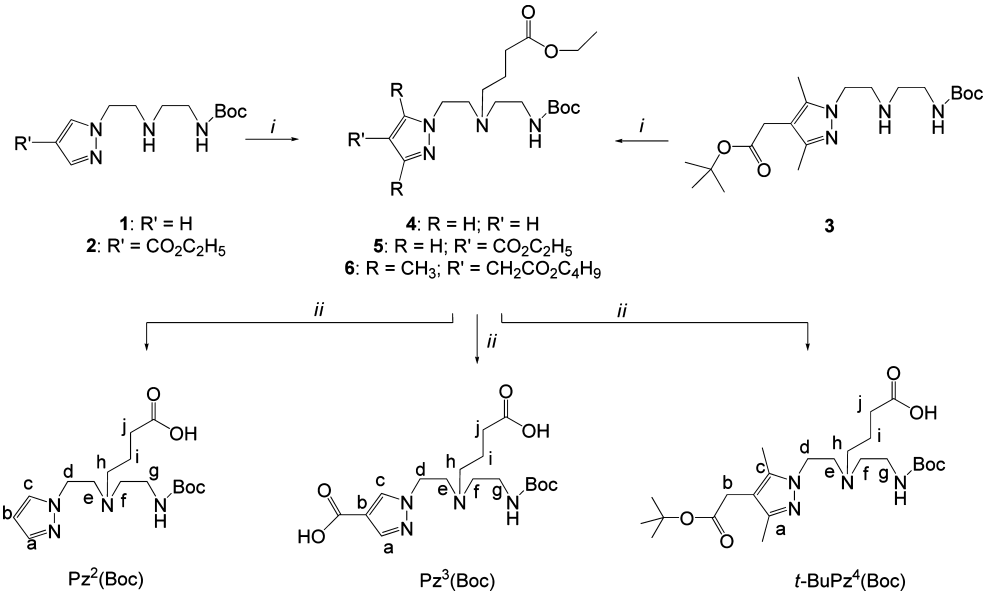

[a](i) $Br(CH_2)_3CO_2Et$, K_2CO_3, KI, CH_3CN; (ii) NaOH, THF/H_2O, rt, overnight; (identification system for NMR assignments is displayed).

Scheme 2. Synthesis of the Peptide Conjugates[a]

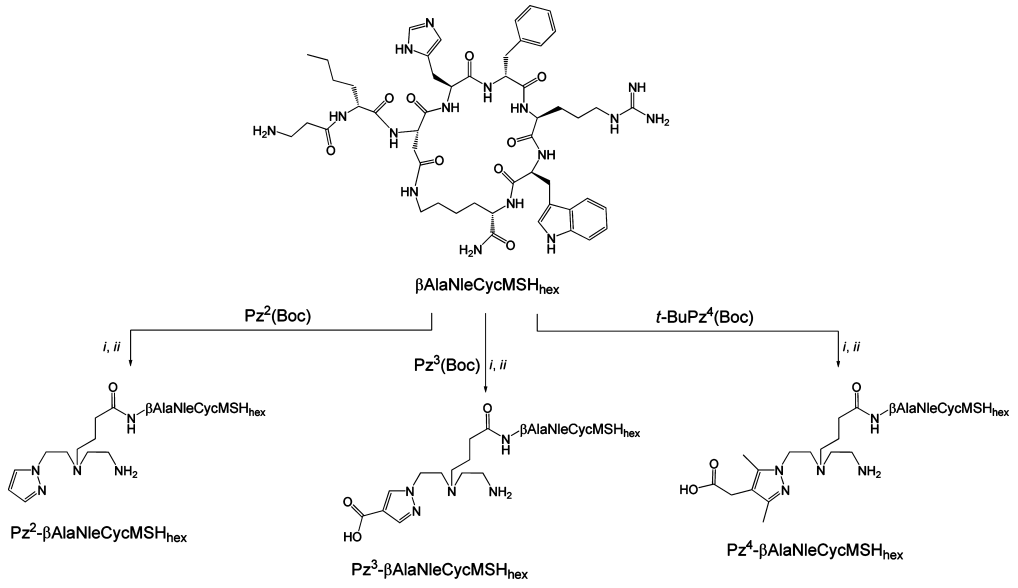

[a](i) HATU, DIPEA, *N,N*-dimethylformamide (DMF); (ii) 95% TFA, 2.5%, triisopropylsilane (TIS), 2.5% H_2O.

Table 1. Analytical Data and Binding Affinity for the α-MSH Derivatives

compd	calcd exact mass (Da)	found calcd [ion]	molecular formula	MC1R affinity (nM)	t_R[a] (min)/ purity	t_R[a] for ^{99m}Tc-conjugate (min)/purity	log $P_{o/w}$ for ^{99m}Tc-conjugate
βAlaNleCycMSH$_{hex}$	1052.60	1053.6 $[M + H]^+$	$C_{51}H_{72}N_{16}O_9$	0.05 ± 0.02	na	na	na
Pz^1-βAlaNleCycMSH$_{hex}$[12]	1302.80	1303.8 $[M + H]^+$	$C_{64}H_{94}N_{20}O_{10}$	0.21 ± 0.05	na	na	+0.19 ± 0.01
Pz^2-βAlaNleCycMSH$_{hex}$	1274.50	638.4 $[M + 2H]^{2+}$	$C_{62}H_{90}N_{20}O_{10}$	0.02 ± 0.01	13.3 (98%)	19.0 (98%)	−0.93 ± 0.01
Pz^3-βAlaNleCycMSH$_{hex}$	1318.70	440.8 $[M + 3H]^{3+}$	$C_{63}H_{90}N_{20}O_{12}$	0.04 ± 0.01	12.7 (98%)	17.9 (98%)	−1.11 ± 0.02
Pz^4-βAlaNleCycMSH$_{hex}$	1360.80	681.8 $[M + 2H]^{2+}$	$C_{66}H_{96}N_{20}O_{12}$	0.16 ± 0.10	11.2 (98%)	17.9 (98%)	−0.88 ± 0.04

[a]gradient D (see Experimental Section); na: not applicable.

dx.doi.org/10.1021/jm301647t | *J. Med. Chem.* 2013, 56, 1961−1973

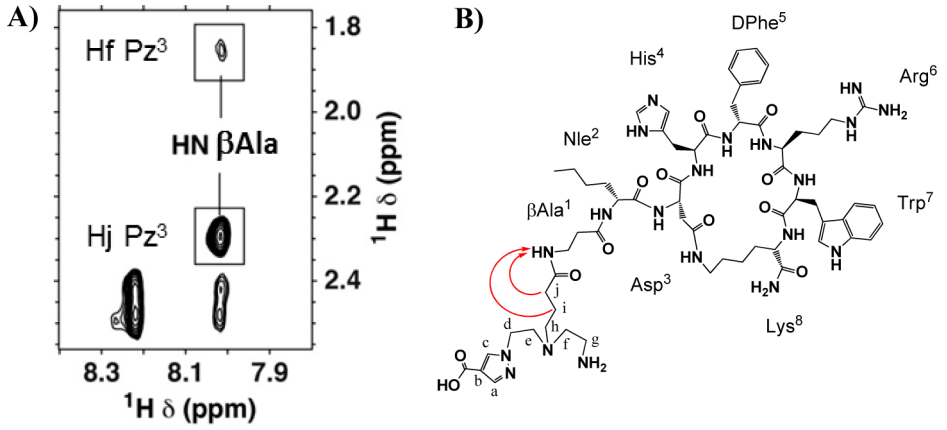

Figure 3. (A) Selected ROESY spectral region of Pz^3-βAlaNleCycMSH$_{hex}$ in aqueous solution (H_2O/D_2O 9/1 v/v) at pH 2.5 and 25 °C. (B) Key correlations observed between Pz^3 and the NH of βAla (red arrow).

further support to this conclusion was attained from the ROE cross-peaks observed between Pz^3 and the peptide moiety that involve protons from the aliphatic arm of Pz^3 but not from the pyrazolyl ring. The observed ROE cross-peaks were a strong cross-peak between the H^j protons of Pz^3 and the HN amide of βAla^1, a medium-weak cross-peak between the H^i protons of Pz^3 and the HN amide of βAla^1, and a weak cross-peak between the H^j protons of Pz^3 and the H_α proton of βAla^1 (Figure 3). None of the ROE cross-peaks expected for the peptide moiety if conjugated through the carboxylate at the pyrazolyl ring were present.

Brought together, the NMR parameters (ROEs and ^{13}C chemical shifts) demonstrated that the conjugation to the peptide occurs by the carboxylate group of the central amine (Supporting Information Tables ST1 and ST2).

Determination of the MC1R Binding Affinities. The binding affinities of the cyclic α-MSH derivatives to the MC1R were evaluated in a competition binding assay in B16F1 cells, using [^{125}I]-NDP-αMSH as radioligand. The IC_{50} values for the peptide conjugates as well as for βAlaNleCycMSH$_{hex}$ are listed in Table 1.

The conjugation of the chelators Pz^2–Pz^4 to βAlaNleCycMSH$_{hex}$ (IC_{50} = 0.05 ± 0.02 nM) led to a slight improvement of the binding affinity in the case of Pz^2-βAlaNleCycMSH$_{hex}$ (IC_{50} = 0.02 ± 0.01 nM) and Pz^3-βAlaNleCycMSH$_{hex}$ (IC_{50} = 0.04 ± 0.01 nM) and a slight decrease in the case of the peptide conjugates Pz^1-βAlaNleCycMSH$_{hex}$ (IC_{50} = 0.21 ± 0.05 nM) and Pz^4-βAlaNleCycMSH$_{hex}$ (IC_{50} = 0.16 ± 0.1nM). Nevertheless, in all cases, the IC_{50} values are of the same order of magnitude as that obtained for the precursor peptide βAlaNleCycMSH$_{hex}$.

Radiolabeling of the Peptide Conjugates. Reaction of the peptide conjugates Pz^2-βAlaNleCycMSH$_{hex}$–Pz^4-βAlaNleCycMSH$_{hex}$ with the organometallic precursor *fac*-[^{99m}Tc(CO)$_3$(H$_2$O)$_3$]$^+$ gave the radiometalated peptides ^{99m}Tc(CO$_3$)-Pz^2-βAlaNleCycMSH$_{hex}$–^{99m}Tc(CO$_3$)-Pz^4-βAlaNleCycMSH$_{hex}$. The radiopeptides were analyzed by RP-HPLC (gradient C) and the chromatograms of Pz^2-βAlaNleCycMSH$_{hex}$ (retention time, t_R = 11.9 min), Pz^3-βAlaNleCycMSH$_{hex}$ (t_R = 10.6 min), and Pz^4-βAlaNleCycMSH$_{hex}$ (t_R = 11.2 min) present only one species, and no precursor (t_R = 15.2 min) or any other radiochemical species could be detected.

To increase the specific activity of the radiopeptides, ^{99m}Tc(CO$_3$)-Pz^2-βAlaNleCycMSH$_{hex}$–^{99m}Tc(CO$_3$)-Pz^4-βAlaNleCycMSH$_{hex}$ were separated from the respective nonlabeled peptide conjugates by RP-HPLC.

Partition Coefficients of the Radiopeptides. The partition coefficients, expressed in log $P_{o/w}$, have been determined for ^{99m}Tc(CO$_3$)-Pz^2-βAlaNleCycMSH$_{hex}$–^{99m}Tc(CO$_3$)-Pz^4-βAlaNleCycMSH$_{hex}$ by the "shake flask" method in physiological conditions (Table 1).[24] The log $P_{o/w}$ values demonstrate the hydrophilic nature of the novel radiometalated peptides, with complex ^{99m}Tc(CO$_3$)-Pz^3-βAlaNleCycMSH$_{hex}$ (log $P_{o/w}$ = −1.11) displaying the highest hydrophilic character.

in Vitro Stability Studies. To assess the resistance of radiocomplexes ^{99m}Tc(CO$_3$)-Pz^2-βAlaNleCycMSH$_{hex}$–^{99m}Tc(CO$_3$)-Pz^4-βAlaNleCycMSH$_{hex}$ to proteolytic degradation caused by endogenous peptidases, stability assays in human serum at 37 °C were performed. Analysis by RP-HPLC at different time points postincubation indicated high serum stability with negligible degradation. As an illustrative example, Figure 4 depicts the RP-HPLC chromatographic profile of ^{99m}Tc(CO$_3$)-Pz^3-βAlaNleCycMSH$_{hex}$ during the assay.

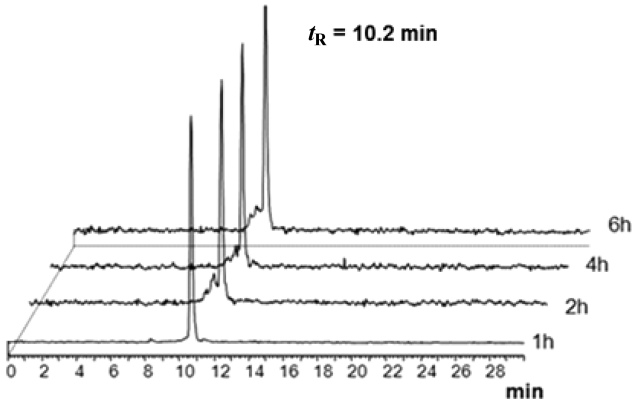

Figure 4. RP-HPLC chromatograms of ^{99m}Tc(CO$_3$)-Pz^3-βAlaNleCycMSH$_{hex}$ after incubation in human serum at different time points (37 °C).

The complexes ^{99m}Tc(CO$_3$)-Pz^2-βAlaNleCycMSH$_{hex}$–^{99m}Tc(CO$_3$)-Pz^4-βAlaNleCycMSH$_{hex}$ were also stable in cysteine and histidine solutions because no degradation or trans-chelation products were observed even after 6 h incubation at 37 °C.

Internalization and Cellular Retention Studies. Aiming to predict the tumor-targeting properties of ^{99m}Tc(CO$_3$)-Pz^2-

dx.doi.org/10.1021/jm301647t | J. Med. Chem. 2013, 56, 1961–1973

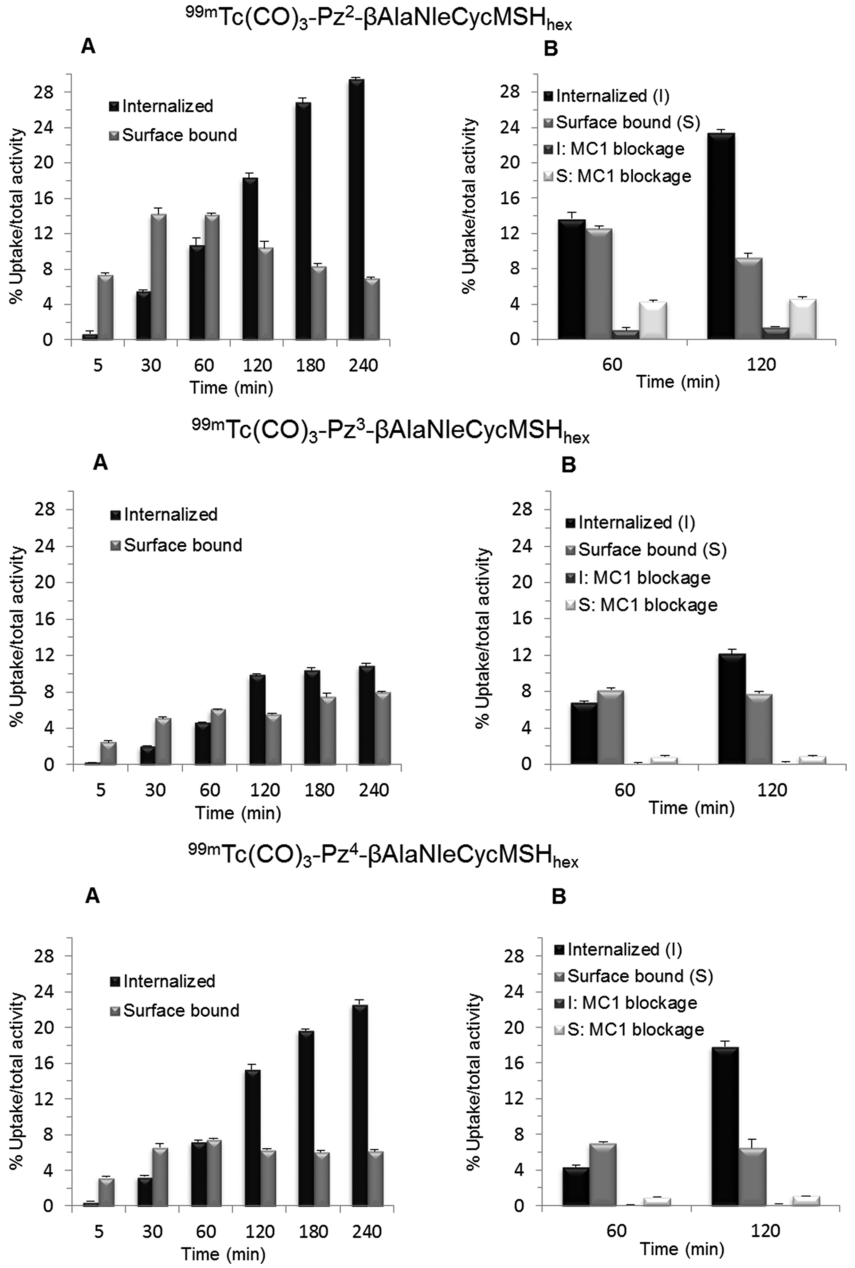

Figure 5. (A) Internalization of the radioconjugates $^{99m}Tc(CO_3)$-Pz^2-βAlaNleCycMSH$_{hex}$–$^{99m}Tc(CO_3)$-Pz^4-βAlaNleCycMSH$_{hex}$ in B16F1 murine melanoma cells at different time points at 37 °C. (B) Effect of MC1R-saturation with NDP-MSH (3.5 μg/well) on the internalized and the surface bound radioconjugates. Internalized and surface bound activity expressed as a percentage of total activity.

βAlaNleCycMSH$_{hex}$–$^{99m}Tc(CO_3)$-Pz^4-βAlaNleCycMSH$_{hex}$, internalization studies in B16F1 murine melanoma cells have been performed at 37 °C, and the results are presented in Figure 5.

The radioconjugates $^{99m}Tc(CO_3)$-Pz^2-βAlaNleCycMSH$_{hex}$–$^{99m}Tc(CO_3)$-Pz^4-βAlaNleCycMSH$_{hex}$ exhibited high levels of time-dependent internalization. The highest level was reached for complex $^{99m}Tc(CO_3)$-Pz^2-βAlaNleCycMSH$_{hex}$ at 4 h postincubation (37 °C) with 29.4 ± 0.3% of the total activity applied internalized in B16F1 cells, corresponding to 81.0 ± 0.4% of the cell-associated activity (Figure 5A). At the same time point, 10.8 ± 0.3% and 22.6 ± 0.5% of the applied activity of $^{99m}Tc(CO_3)$-Pz^3-βAlaNleCycMSH$_{hex}$ and $^{99m}Tc(CO_3)$-Pz^4-βAlaNleCycMSH$_{hex}$ was internalized in B16F1 cells, corresponding to 57.8 ± 0.5% and 78.6 ± 0.4% of cellular uptake of $^{99m}Tc(CO_3)$-Pz^3-βAlaNleCycMSH$_{hex}$ and $^{99m}Tc(CO_3)$-Pz^4-βAlaNleCycMSH$_{hex}$, respectively.

To evaluate the specificity of cellular uptake, internalization studies of $^{99m}Tc(CO_3)$-Pz^2-βAlaNleCycMSH$_{hex}$–$^{99m}Tc(CO_3)$-Pz^4-βAlaNleCycMSH$_{hex}$ in B16F1 cells at 1 h and 2 h (37 °C) were also performed with coincubation with NDP-MSH (3.5 μg/well), a α-MSH analogue with high affinity for MC1R (0.21 nM). In vitro MC1R-saturation data is represented in Figure 5B. In the presence of NDP-MSH, the internalization of all radioconjugates was strongly inhibited, being almost complete for $^{99m}Tc(CO_3)$-Pz^3-βAlaNleCycMSH$_{hex}$ and $^{99m}Tc(CO_3)$-Pz^4-βAlaNleCycMSH$_{hex}$, with a reduction of 99% of internalized activity at 2 h postincubation versus 94% for $^{99m}Tc(CO_3)$-Pz^2-βAlaNleCycMSH$_{hex}$. The cell surface-bound activity of ^{99m}Tc-

dx.doi.org/10.1021/jm301647t | J. Med. Chem. 2013, 56, 1961−1973

(CO_3)-Pz^3-βAlaNleCycMSH$_{hex}$ and ^{99m}Tc(CO_3)-Pz^4-βAlaNleCycMSH$_{hex}$ was also highly reduced in the presence of NDP-MSH (90% and 87% of inhibition after 1 h; 89% and 84% of inhibition after 2 h, respectively). Lower inhibition values were found for ^{99m}Tc(CO_3)-Pz^2-βAlaNleCycMSH$_{hex}$ (66% and 50% at 1 h and 2 h, respectively), indicating a higher nonspecific binding to cell membrane.

The cellular retention of ^{99m}Tc(CO_3)-Pz^2-βAlaNleCycMSH$_{hex}$–^{99m}Tc(CO_3)-Pz^4-βAlaNleCycMSH$_{hex}$ was evaluated at different time points after 3 h internalization in B16F1 cells at 37 °C (Figure 6). Good retention values were found for all compounds, and ^{99m}Tc(CO_3)-Pz^4-βAlaNleCycMSH$_{hex}$ presented the best value with 62% of the internalized activity still remaining inside the cells after 4 h. Complexes ^{99m}Tc(CO_3)-Pz^2-βAlaNleCycMSH$_{hex}$ and ^{99m}Tc(CO_3)-Pz^3-βAlaNleCycMSH$_{hex}$ presented a similar behavior, with 48% and 50% of the internalized activity retained in the cells.

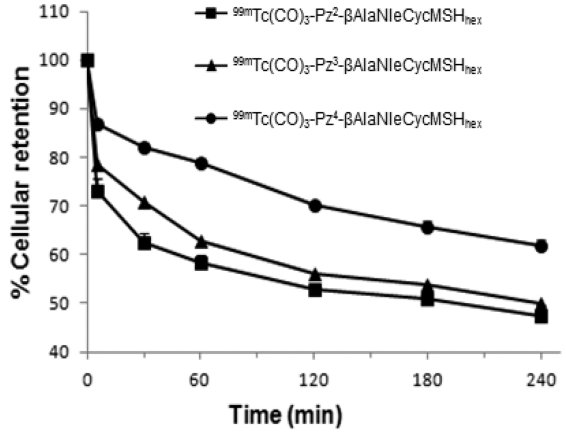

Figure 6. Cellular retention of internalized radioconjugates ^{99m}Tc(CO_3)-Pz^2-βAlaNleCycMSH$_{hex}$–^{99m}Tc(CO_3)-Pz^4-βAlaNleCycMSH$_{hex}$ in B16F1 melanoma cells over time at 37 °C.

Biodistribution Studies. The in vivo MC1R-targeting properties of radiopeptides were evaluated in B16F1 melanoma-bearing mice. Table 2 presents the tissue distributions of the ^{99m}Tc(CO_3)-Pz^2-βAlaNleCycMSH$_{hex}$–^{99m}Tc(CO_3)-Pz^4-βAlaNleCycMSH$_{hex}$ in comparison with the previously reported radiopeptide ^{99m}Tc(CO_3)-Pz^1-βAlaNleCycMSH$_{hex}$,[12] at 1 h and 4 h pi, as well as the data corresponding to radioconjugates ^{99m}Tc(CO_3)-Pz^3-βAlaNleCycMSH$_{hex}$ and ^{99m}Tc(CO_3)-Pz^4-βAlaNleCycMSH$_{hex}$ coinjected with 20 μg/mice of NDP-MSH.

All radiopeptides exhibited rapid, high, and comparable tumor uptake at 1 h pi, with 11.82 ± 3.91% IA/g for ^{99m}Tc$(CO)_3$-Pz^3-βAlaNleCycMSH$_{hex}$, 10.55 ± 1.83% IA/g for ^{99m}Tc$(CO)_3$-Pz^4-βAlaNleCycMSH$_{hex}$, and 9.90 ± 1.10% IA/g for ^{99m}Tc$(CO)_3$-Pz^2-βAlaNleCycMSH$_{hex}$. At 4 h post injection, ^{99m}Tc$(CO)_3$-Pz^2-βAlaNleCycMSH$_{hex}$ displayed the highest tumor uptake (9.51 ± 1.34% IA/g).

For all the radiopeptides, the liver and kidney uptake values were significantly lower than the ones previously described for complex ^{99m}Tc$(CO)_3$-Pz^1-βAlaNleCycMSH$_{hex}$.[12] However, the radiocompounds ^{99m}Tc$(CO)_3$-Pz^3-βAlaNleCycMSH$_{hex}$ and ^{99m}Tc$(CO)_3$-Pz^4-βAlaNleCycMSH$_{hex}$ have shown the best biological profile.

To evaluate the in vivo MC1R-binding specificity of ^{99m}Tc(CO_3)-Pz^3-βAlaNleCycMSH$_{hex}$ and ^{99m}Tc(CO_3)-Pz^4-βAlaNleCycMSH$_{hex}$, the radioconjugates were coadministrated with cold NDP-MSH (20 μg/mice) in B16F1 melanoma-bearing mice.

As expected, the MC1R-saturation with this potent agonist leads to a considerable reduction in the tumor uptake of ^{99m}Tc(CO_3)-Pz^3-βAlaNleCycMSH$_{hex}$ (from 11.82 ± 3.91% to 4.15 ± 0.53% IA/g) and ^{99m}Tc(CO_3)-Pz^4-βAlaNleCycMSH$_{hex}$ (from 10.55 ± 1.83% to 2.35 ± 0.46% IA/g), without significant changes in the biodistribution profile of the radioconjugates in normal tissues.

Because of the favorable pharmacokinetics of ^{99m}Tc(CO_3)-Pz^3-βAlaNleCycMSH$_{hex}$ and ^{9m}Tc(CO_3)-Pz^4-βAlaNleCycMSH$_{hex}$, their melanoma imaging properties were further evaluated. Figure 7 presents planar scintigraphic images of B16F1 murine melanoma-bearing C57BL/6 mice injected with ^{99m}Tc(CO_3)-Pz^3-βAlaNleCycMSH$_{hex}$ and ^{99m}Tc(CO_3)-Pz^4-βAlaNleCycMSH$_{hex}$ at 1 h pi. Melanoma was clearly visualized with high contrast between tumor and background. Images are consistent with the biodistribution results, showing a lower liver uptake for ^{99m}Tc$(CO)_3$-Pz^3-βAlaNleCycMSH$_{hex}$ and a lower kidney uptake for ^{99m}Tc$(CO)_3$-Pz^4-βAlaNleCycMSH$_{hex}$.

The analysis of tissue samples collected from the sacrificed mice at 1 h and 4 h pi has shown that all radiopeptides were stable in blood serum, tumor, and liver homogenates (Supporting Information SM6), as no metabolites could be detected after 4 h pi. However, after 4 h pi, new species with lower retention time, corresponding to hydrophilic metabolites (not identified), were detected in kidney homogenate (Supporting Information SM6) and urine. As an example, Figure 8 displays the RP-HPLC profile of ^{99m}Tc(CO_3)-Pz^3-βAlaNleCycMSH$_{hex}$ and the corresponding blood and urine samples at 1 h and 4 h pi.

DISCUSSION

In our continued effort to design radioactive probes for melanoma imaging, we have assessed the MC1R-targeting properties of ^{99m}Tc$(CO)_3$-labeled radiolabeled linear and cyclic derivatives of α-MSH.[11,12,25−27] We have already demonstrated the advantages of lactam bridge-cyclization on melanoma uptake, and herein our goal was to improve the overall biological profile of ^{99m}Tc$(CO)_3$-labeled βAlaNleCycMSH$_{hex}$ through structural modification of the azolyl ring of the pyrazolyl-diamine chelator. The three pyrazole-diamine chelators selected (Pz^2(Boc)–Pz^4(Boc)) allowed the preparation of hydrophilic complexes when compared to Pz^1(Boc) (data not shown).[12] The chelators Pz^1 and Pz^4 contain methyl groups at the 3- and 5-positions of the azolyl ring, with Pz^4 presenting an extra methylene carboxylate arm at the 4-position. Pz^2 has no substituent groups at all on the ring, whereas Pz^3 holds a carboxylate directly attached to the 4-position of the azolyl ring.

The conjugation of the different Pz chelators to the N-terminus of βAlaNleCycMSH$_{hex}$ did not disturb its MC1R-binding properties, as indicated by the subnanomolar IC_{50} values found for all peptide conjugates (Table 1).

The radiometalated peptides ^{99m}Tc$(CO)_3$-Pz^2-βAlaNleCycMSH$_{hex}$–^{99m}Tc$(CO)_3$-Pz^4-βAlaNleCycMSH$_{hex}$ presented high in vitro stability, confirming the radiopeptide resistance to proteolytic degradation caused by endogenous peptidases, and the high ability of the pyrazolyl-diamine unit to stabilize the core *fac*-[^{99m}Tc$(CO)_3$]$^+$, without transmetalation

dx.doi.org/10.1021/jm301647t | J. Med. Chem. 2013, 56, 1961−1973

Table 2. Biodistribution Studies of $^{99m}Tc(CO)_3$-Pz^1-βAlaNleCycMSH$_{hex}$–$^{99m}Tc(CO)_3$-Pz^4-βAlaNleCycMSH$_{hex}$ in B16F1 Murine Melanoma-Bearing C57BL/6 Mice at 1 h and 4 h pi (n = 3–5)

	% IA/g ± SD									
	$^{99m}Tc(CO)_3$-Pz^1-βAlaNleCycMSH$_{hex}$[12]		$^{99m}Tc(CO)_3$-Pz^2-βAlaNleCycMSH$_{hex}$		$^{99m}Tc(CO)_3$-Pz^3-βAlaNleCycMSH$_{hex}$			$^{99m}Tc(CO)_3$-Pz^4-βAlaNleCycMSH$_{hex}$		
tissue/organ	1 h	4 h	1 h	4 h	1 h	4 h	1 h with NDP[a]	1 h	4 h	1 h with NDP[a]
tumor	9.26 ± 0.83	11.31 ± 1.83	9.90 ± 1.10	9.51 ± 1.34	11.82 ± 3.91	4.15 ± 0.53	1.69 ± 0.02	10.55 ± 1.83	6.15 ± 1.00	2.35 ± 0.46
blood	2.71 ± 0.64	1.67 ± 0.24	1.82 ± 0.05	0.77 ± 0.09	0.65 ± 0.14	0.49 ± 0.01	0.84 ± 0.10	0.92 ± 0.05	0.41 ± 0.06	2.80 ± 0.64
liver	42.19 ± 5.05	22.86 ± 1.17	23.97 ± 3.67	7.09 ± 0.42	2.96 ± 1.15	1.87 ± 0.17	4.33 ± 0.25	5.08 ± 0.12	2.13 ± 0.23	6.69 ± 1.46
intestine	5.17 ± 0.91	8.45 ± 0.76	8.24 ± 1.04	10.59 ± 2.78	0.84 ± 0.26	1.60 ± 0.31	0.99 ± 0.36	2.28 ± 0.11	3.87 ± 0.54	1.81 ± 0.37
spleen	2.54 ± 0.28	2.24 ± 0.37	7.67 ± 0.66	3.91 ± 0.38	0.44 ± 0.05	0.24 ± 0.03	0.83 ± 0.41	0.65 ± 0.04	0.28 ± 0.08	1.77 ± 0.73
heart	1.04 ± 0.19	0.48 ± 0.07	2.85 ± 0.16	1.25 ± 0.07	0.29 ± 0.02	0.24 ± 0.09	0.51 ± 0.08	0.33 ± 0.11	0.15 ± 0.03	1.41 ± 0.40
lung	3.85 ± 0.46	1.54 ± 0.16	7.16 ± 1.47	3.23 ± 0.59	0.78 ± 0.07	0.24 ± 0.09	0.57 ± 0.65	0.91 ± 0.19	0.31 ± 0.03	2.65 ± 0.83
kidney	71.06 ± 6.44	32.12 ± 1.57	24.86 ± 1.80	4.02 ± 0.17	7.72 ± 1.33	2.97 ± 0.28	13.03 ± 1.19	2.98 ± 0.59	0.87 ± 0.14	9.83 ± 4.29
muscle	0.35 ± 0.07	0.19 ± 0.08	0.49 ± 0.05	0.15 ± 0.01	0.16 ± 0.02	0.05 ± 0.01	0.25 ± 0.07	0.17 ± 0.01	0.04 ± 0.02	0.69 ± 0.30
bone	1.14 ± 0.19	0.70 ± 0.13	0. 99 ± 0.09	0.39 ± 0.03	0.33 ± 0.02	0.16 ± 0.06	0.45 ± 0.11	0.43 ± 0.20	0.11 ± 0.01	0.93 ± 0.25
stomach	1.97 ± 0.75	0.88 ± 0.46	2.92 ± 0.72	0.32 ± 0.10	1.12 ± 0.39	0.07 ± 0.00	1.08 ± 0.17	1.32 ± 0.38	0.18 ± 0.07	1.69 ± 0.11
pancreas	0.73 ± 0.32	0.39 ± 0.10	0.76 ± 0.05	0.26 ± 0.06	0.22 ± 0.02	0.09 ± 0.00	0.43 ± 0.08	0.16 ± 0.02	0.07 ± 0.02	0.98 ± 0.17
Tumor:Normal Tissue Uptake Ratio										
tumor:blood	3.4	6.8	5.4	12.3	18.2	8.5		11.5	15	
tumor: muscle	26.5	61.4	20.2	63.4	73.9	83.0		62	153.7	
tumor:kidney	0.13	0.35	0.40	2.36	1.53	1.4		3.5	7.1	
tumor:liver	0.22	0.49	0.41	1.34	3.99	2.2		2.08	2.89	
total excretion (%)	14.2 ± 2.3	37.4 ± 2.4	27.6 ± 1.3	56.5 ± 7.0	73.9 ± 1.9	69.7 ± 1.7	63.4 ± 8.3	74.3 ± 2.4	83.7 ± 2.8	36.2 ± 22.6

[a]Coinjection of the radioconjugate with NDP-MSH.

dx.doi.org/10.1021/jm301647t | J. Med. Chem. 2013, 56, 1961–1973

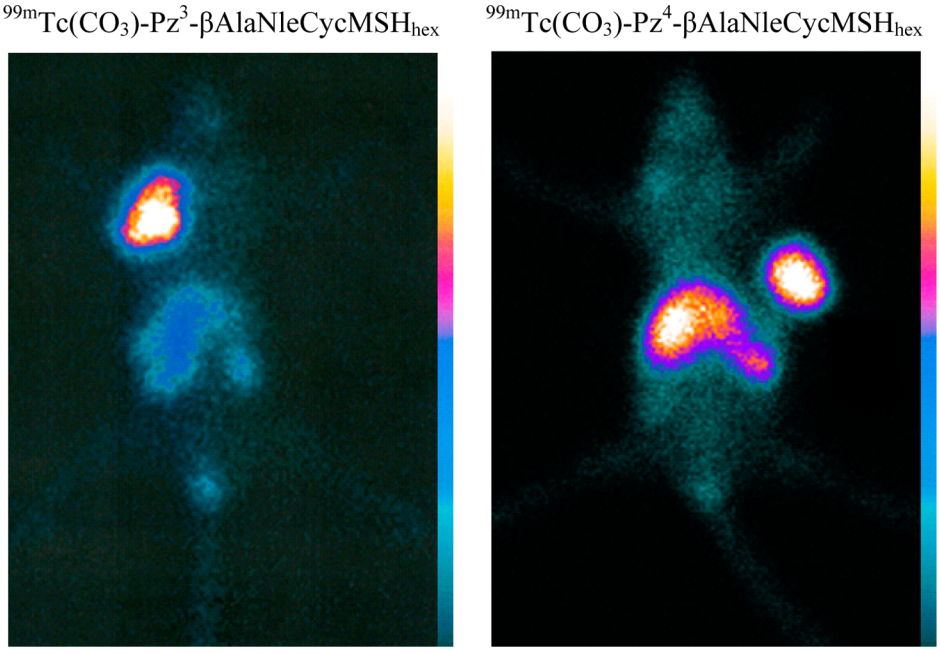

Figure 7. Planar scintigraphic images of B16F1 murine melanoma-bearing C57BL/6 mice injected with ^{99m}Tc(CO$_3$)-Pz^3-*β*AlaNleCycMSH$_{hex}$ and ^{99m}Tc(CO$_3$)-Pz^4-*β*AlaNleCycMSH$_{hex}$ at 1 h pi.

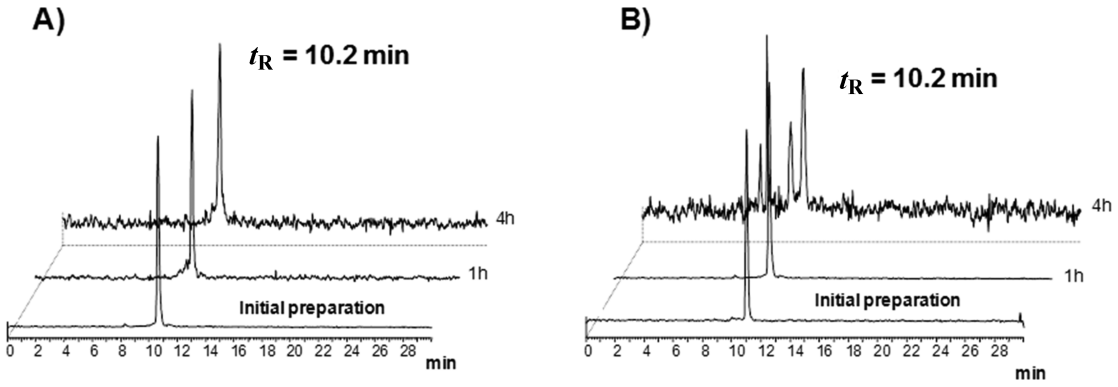

Figure 8. RP-HPLC *γ* traces of ^{99m}Tc(CO$_3$)-Pz^3-*β*AlaNleCycMSH$_{hex}$ (initial preparation), blood serum (A), and urine samples (B) collected 1 h and 4 h after injection.

to serum-based proteins or amino acids and/or reoxidation to ^{99m}Tc(VII).

Internalization studies in murine B16F1 melanoma cells have shown that cellular uptake of ^{99m}Tc(CO)$_3$-Pz^2-*β*AlaNleCycMSH$_{hex}$–^{99m}Tc(CO)$_3$-Pz^4-*β*AlaNleCycMSH$_{hex}$ was MC1R-mediated, suggesting that the affinity of the radiopeptides was preserved upon radiometalation. Indeed, the radiopeptides displayed high level of time-dependent internalization in murine B16F1 melanoma cells which was strongly inhibited (92−99%) by receptor saturation with NDP-MSH (IC_{50} = 0.21 nM).

The in vivo MC1R-targeting properties of the radiopeptides were evaluated in B16F1 melanoma-bearing mice. High melanoma uptake (ca. 10% IA/g) was observed for all radiopeptides at 1 h pi, being the values comparable to the one found for the previously reported radiopeptide ^{99m}Tc(CO)$_3$-Pz^1-*β*AlaNleCycMSH$_{hex}$ (9.26 ± 0.83% IA/g).[12] However, the structural modification in the azolyl ring substitution pattern of the chelator had a profound effect on the pharmacokinetic profile of the radiopeptides.

Indeed, the absence of the methyl groups in the azolyl ring of ^{99m}Tc(CO)$_3$-Pz^2-*β*AlaNleCycMSH$_{hex}$ not only reduced significantly the kidney and liver accumulation (87% and 69%, respectively, at 4 h pi) but also increased the total activity excreted by urinary route (51%, at 4h pi) when compared with ^{99m}Tc(CO)$_3$-Pz^1-*β*AlaNleCycMSH$_{hex}$. Nevertheless, the pharmacokinetic profile of ^{99m}Tc(CO)$_3$-Pz^2-*β*AlaNleCycMSH$_{hex}$ was not still adequate for efficient melanoma imaging due to a reasonable accumulation of the radiopeptide in the liver and kidney (4.02 ± 0.17 and 7.09 ± 0.42% IA/g, respectively) at 4 h pi.

The radiopeptides ^{99m}Tc(CO)$_3$-Pz^3-*β*AlaNleCycMSH$_{hex}$ and ^{99m}Tc(CO)$_3$-Pz^4-*β*AlaNleCycMSH$_{hex}$ presented a striking kidney and liver uptake reduction (>90%, at 4 h pi) upon comparison with ^{99m}Tc(CO)$_3$-Pz^1-*β*AlaNleCycMSH$_{hex}$. Moreover, the overall radioactivity elimination of both radiopeptides occurred mainly through the renal pathway, and the whole-body clearance was faster than that observed for ^{99m}Tc(CO)$_3$-Pz^1-*β*AlaNleCycMSH$_{hex}$, or ^{99m}Tc(CO)$_3$-Pz^2-*β*AlaNleCycMSH$_{hex}$. This shift from hepatobiliary toward renal

excretion pathway as well as the faster clearance of ^{99m}Tc-(CO)$_3$-Pz^3-βAlaNleCycMSH$_{hex}$ and ^{99m}Tc(CO)$_3$-Pz^4-βAlaNle-CycMSH$_{hex}$ could be ascribed to a reduction of the net positive charge of the radiopeptides due to the presence of a carboxylate group in the pyrazolyl ring of the chelator.

The favorable biodistribution profile of ^{99m}Tc(CO)$_3$-Pz^3-βAlaNleCycMSH$_{hex}$ and ^{99m}Tc(CO)$_3$-Pz^4-βAlaNleCycMSH$_{hex}$ allowed a clear visualization of flank melanoma lesions in tumor-bearing mice by SPECT-imaging at 1 h pi. Moreover, an enhanced tumor-to-kidney and tumor-to-liver ratios for both compounds generated high contrast between tumor and background.

In comparison with lactam bridge-cyclized radiopeptides reported by others, ^{99m}Tc(CO)$_3$-Pz^3-βAlaNleCycMSH$_{hex}$ and ^{99m}Tc(CO)$_3$-Pz^4-βAlaNleCycMSH$_{hex}$ presented lower tumor uptake and tumor/liver ratios values than ^{67}Ga-NOTA-GlyGlyNle-CycMSHhex. However, very high tumor/kidney ratios values were found at 4 h pi for ^{99m}Tc(CO)$_3$-Pz^4-βAlaNleCycMSH$_{hex}$ (7.1). Indeed, this radiopeptide presented a 2.4−50-fold enhancement of tumor:kidney ratios when compared with other lactam-based cyclic radiopeptides, like ^{111}In-DOTA-Nle-CycMSH$_{hex}$ (1.70), Ac-GluGlu-CycMSH-[DOTA]-^{111}In (0.14), ^{111}In-DOTA-GlyGlyNle-CycMSH$_{hex}$ (2.73), ^{111}In-DOTA-GlyGluNle-CycMSH$_{hex}$ (0.85), ^{67}Ga-DOTA-GlyGlu-CycMSH (0.36), ^{67}Ga-DOTA-GlyGlyNle-CycMSH$_{hex}$ (2.98), and ^{67}Ga-NOTA-GlyGlyNle-CycMSH$_{hex}$ (2.40), at 4 h pi.[7−10,28]

CONCLUSION

Taken together, the results highlight the ability of different pyrazolyl-diamine-type chelators to tune the pharmacokinetic properties of ^{99m}Tc(CO)$_3$-labeled peptides, namely α-MSH derivatives, without compromising their in vitro and in vivo targeting properties. Indeed, this study demonstrated that structural modifications on the chelating system, particularly the introduction of carboxylate groups shifts the excretion pathway of a radiopeptide from mainly hepatobiliar toward mainly renal and, simultaneously, improves notably tumor-to-nontarget-organs ratios. The relevant biological properties of ^{99m}Tc(CO)$_3$-Pz^3-βAlaNleCycMSH$_{hex}$ and ^{99m}Tc(CO)$_3$-Pz^4-βAlaNleCycMSH$_{hex}$ demonstrated at the preclinical level, namely the good tumor uptake and favorable tumor-to-nontarget-organs ratios highlights the potential usefulness of both compounds as melanoma imaging agents. Additionally, other improvements based on structural modifications can still be envisaged due to the versatility of the chelating system.

EXPERIMENTAL SECTION

Material and Methods. All the Fmoc-amino acids were a gift from CEM while Fmoc-Asp(Dmab), and Fmoc-Lys(ivDde), Rink Amide resin, and HATU were purchased from Novabiochem (Merck, Lisbon, Portugal).

^{1}H and ^{11}C NMR spectra of the BFCs were recorded at room temperature on a Varian Unity 300 MHz spectrometer. ^{1}H and ^{13}C chemical shifts were referenced with the residual solvent resonances relatively to tetramethylsilane. The spectra were assigned based on 2D experiments (^{1}H−^{1}H correlation spectroscopy, COSY). Assignments of the ^{1}H and ^{13}C NMR peaks are given in accordance with the identification system shown in Scheme 1. Infrared spectra were recorded as KBr pellets on a Bruker Tensor 27 spectrometer. The purity of all tested compounds was ≥95%, as confirmed by HPLC analysis.

NDP-MSH was purchased from Neosystem (Strasbourg, France). Bovine serum albumin (BSA) was purchased from Sigma. Dulbecco's Modified Eagle's Medium (DMEM) containing GlutaMax I, fetal bovine serum, penicillin/streptomycin antibiotic solution, trypsin−EDTA, and phosphate-buffered saline (PBS) pH 7.2 were all from Gibco−Invitrogen (Alfagene, Lisbon).

Reverse Phase High Performance Liquid Chromatography Analysis. HPLC analyses were performed on a Perkin-Elmer LC pump 200 coupled to a Shimadzu SPD 10AV UV/vis and to a Berthold-LB 509 radiometric detector. Analytical control of the BFC's was achieved using an analytical Macherey-Nagel C18 reversed-phase column (Nucleosil 100−10, 250 mm × 4 mm) with a flow rate of 1.0 mL min^{-1}, while purification of the complexes was achieved using a semipreparative Macherey-Nagel C18 reversed-phase column (Nucleosil 100−7, 250 mm × 8 mm) with a flow rate of 2.0 mL min^{-1} (gradient A), respectively. UV detection: 220 nm. Analytical control and semipreparative purifications of the βAlaNleCycMSH$_{hex}$ and peptide conjugates was achieved on Supelco Discovery Bio Wide Pore C18 (250 mm × 4.6 mm, 5 μm) and Supelco Discovery Bio Wide Pore C18 (250 mm × 10 mm, 10 μm)) with a flow rate of 1.0 mL min^{-1} or 2.0 mL min^{-1} (gradient B), respectively.

Analytical control and semipreparative purifications of ^{99m}Tc(CO)$_3$-labeled α-MSH analogues were done on a Hypersil ODS column (250/4 mm, 10 μm) and Hypersil ODS column (250/8 mm, 10 μm) eluted with flow rate of 1.0 mL min^{-1} and 3.0 mL min^{-1} and using gradients C and D, respectively.

Applied Binary Gradients. Gradient A (mobile phase A, TFA 0.1%; mobile phase B, MeOH) 0−3 min, 0% B; 3−3.1 min, 0−25% B; 3.1−9 min, 25% B; 9−9.1 min, 25−34% B; 9.1−20 min, 34−100% B; 20−25 min, 100% B; 25−25.1, 100−0% B; 25.1−30 min, 0% B.

Gradient B (mobile phase A, TFA 0.1%; mobile phase B, CH_3CN 0.1% TFA) 0−50 min, 10−95% B; 50−50.1, 95−100% B; 50.1−54 min, 100% B; 54−55 min, 100−10% B; 55−60 min, 10% B.

Gradient C (mobile phase A, 0.5% TFA; mobile phase B, CH_3CN 0.5% TFA) 0−18 min, 15−100% B; 18−20 min, 100−15% B; 20−30 min, 15% B.

Gradient D (mobile phase A, 0.5% TFA; mobile phase B, CH_3CN 0.5% TFA) 0−5 min, 15−30% B; 5−10 min, 30% B; 10−25 min 30−60% B, 25−28 min 60% B; 28−30 min 60−15% B.

Synthesis of Pz(Boc) Derivatives. *Synthesis of 4-((2-(1H-Pyrazol-1-yl)ethyl)(2-(tert-butoxycarbonylamino)ethyl)amino)-butanoic Acid (Pz^2(Boc)).* Compound was prepared from precursor **1** as described elsewhere.[23] IR (KBr, cm^{-1}): 3421s, 1698 s, 1627s and 1575s. ^{1}H NMR (300 MHz, $CDCl_3$) δ_H: 7.47 (dd, Hpz$^{a/c}$, 1H), 7.43 (dd, Hpz$^{a/c}$, 1H), 6.19 (s, Hpz^b, 1H), 5.06 (br s, NHBoc, 1H), 4.15 (t, CH_2^d, 2H), 3.02 (t, CH_2^g, 2H), 2.86 (t, CH_2^e, 2H), 2.46 (d, CH_2^{f+h}, 4H), 2.14 (br s, CH_2^j, 2H), 3.12), 1.61 (br s, CH_2^i, 2H), 1.40 (s, CH3, 9H). ^{13}C NMR (75.3 MHz, $CDCl_3$) δ_C: 184.7 (CO), 173.2 (CO), 142.9 (C^c), 135.6 (C^a), 122.4 (C^{pz}), 83.1 ($C(CH_3)$) 55.2 (C^j), 54.6 (C^f), 52.3 (C^e), 50.1 (C^d), 39.1 (C^g), 37.1 (C^h), 29.7 ($C(CH_3)$), 24.3 (C^i). RP-HPLC (220 nm, gradient A): 99% (t_R = 16.3 min). ESI-MS (+) (m/z): 341.1 [M + H]$^+$, calcd for $C_{16}H_{28}N_4O_4$ = 340.2.

Synthesis of 1-(2-((2-(*tert*-Butoxycarbonylamino)ethyl)(3-carboxypropyl)amino)ethyl)-1*H*-pyrazole-4-carboxylic Acid (Pz^3(Boc)). *Synthesis of Ethyl 1-(2-((2-(tert-Butoxycarbonylamino)-ethyl)(4-ethoxy-4-oxobutyl)amino)ethyl)-1H-pyrazole-4-carboxylate (5).* The precursor **2** already described elsewhere (0.54 g, 1.7 mmol),[23] ethyl 4-bromobutanoate (0.65 g, 2.4 mmol), K_2CO_3 (0.42 g, 2.4 mmol), and a catalytic amount of KI were dissolved in acetonitrile (20 mL) and allowed to reflux for 18 h. The solution was filtered and vacuum-dried, and the obtained residue was purified by flash chromatography (silica gel, dichloromethane/methanol, 0−5%), giving **5** as a yellowish oil, after removal of the solvent from the collected fractions. Yield: 69% (0.5 g, 1.1 mmol). IR (KBr, cm^{-1}): 3424 s, 1690 s, 1561s and 1414s. ^{1}H NMR (300 MHz, $CDCl_3$) δ_H: 7.92 (s, Hpz, 1H), 7.89 (s, Hpz, 1H), 5.01 (br s, NHBoc, 1H), 4.21 (t, CH_2^d, 2H), 4.12 (q, OCH_2CH_3, 4H), 3.05 (q, CH_2^e, 2H), 2.51 (s, CH_2^f, 2H), 2.44 (q, CH_2^h, 2H), 2.13 (t, CH_2^j, 2H), 1.58 (t, CH_2^i, 2H), 1.42 (s, CH_3, 9H), 1.29 (q, OCH_2CH_3, 6H). ^{13}C NMR (75.3 MHz, $CDCl_3$) δ_C: 173.1 (CO), 162.5 (CO), 155.9 (CO), 140.6 (C^c), 131.7 (C^a), 115.3 (C^{pz}), 80.5 ($C(CH_3)$), 62.1(CH_2CH_3), 61.8 (CH_2CH_3), 59.6 (C^h),

dx.doi.org/10.1021/jm301647t | J. Med. Chem. 2013, 56, 1961−1973

56.4 (C^e), 53.9 (C^f), 51.4 (C^d), 38.8 (C^g), 31.6 (C^j), 28.6 ($C(CH_3)$), 24.4 (C^i), 14.2 (CH_2CH_3).

Synthesis of 1-(2-((2-(tert-Butoxycarbonylamino)ethyl)(3-carboxypropyl)amino)ethyl)-1H-pyrazole-4-carboxylic Acid (Pz^3(Boc)). A solution of NaOH (0.18 g, 0.45 mmol) dissolved in a mixture of H_2O/THF was added to **5** (0.1 g, 0.22 mmol) in THF, and the reaction mixture was stirred overnight at room temperature. After neutralization with hydrochloric acid (1M) at 0 °C and solvent evaporation under reduced pressure, the crude was purified through Sep-Pack C-18 cartridge (water/methanol, 0−100%), giving Pz^3(Boc) as a colorless oil. Yield: 29% (0.03 g; 0.08 mmol). ^{1}H NMR (300 MHz, D_2O) δ_H: 7.84 (s, Hpz, 1H), 7.67 (s, H^{pz}, 1H), 4.16 (t, CH_2^d, 2H), 2.99 (m, $CH_2^{h/f}$, 4H), 2.55 (m, $CH_2^{e/g}$, 4H), 2.01 (s, CH_2^j, 2H), 1.56 (m, CH_2^i, 2H), 1.25 (s, CH_3, 9H). ^{13}C NMR (75.3 MHz, D_2O) δ_C: 184.7 (CO), 173.2 (CO), 160.1 (CO), 142.9 (C^c), 135.6 (C^a), 122.4 (C^{pz}), 83.1 ($C(CH_3)$) 55.2 (C^j), 54.6 (C^f), 52.3 (C^e), 50.1 (C^d), 39.1 (C^g), 37.1 (C^h), 29.7 ($C(CH_3)$), 24.3 (C^i). RP-HPLC (220 nm, gradient A): 99% (t_R = 15.1 min). ESI-MS (+) (m/z): 385.2 [M + H]$^+$, calcd for $C_{17}H_{28}N_4O_6$ = 384.2.

Synthesis of 4-((2-(4-(2-*tert*-Butoxy-2-oxoethyl)-3,5-dimethyl-1*H*-pyrazol-1-yl)ethyl)(2-(*tert*-butoxycarbonylamino)ethyl)amino)butanoic Acid (*t*-BuPz^4(Boc)). *Synthesis of Ethyl 4-((2-(4-(2-tert-Butoxy-2-oxoethyl)-3,5-dimethyl-1H-pyrazol-1-yl)ethyl)(2-(tert-butoxycarbonylamino)ethyl)amino)butanoate (**6**)*. The precursor **3** already described elsewhere (0.54 g, 1.7 mmol),[26] (0.40 g, 1.00 mmol), ethyl 4-bromobutanoate (0.39 g, 2.00 mmol), K_2CO_3 (0.28, 2.00 mmol), and a catalytic amount of KI were dissolved in acetonitrile (10 mL), and the resulting mixture allowed to reflux for 18 h. The solution was filtered and vacuum-dried, and the residue was purified by flash chromatography (silica gel, ethyl acetate/methanol, 0−15%), giving **6** as a yellowish oil. Yield: 45% (0.23 g, 0.45 mmol). ^{1}H NMR (300 MHz, $CDCl_3$) δ_H: 5.34 (br s, NHBoc, 1H), 4.07 (q, OCH_2CH_3, 2H), 3.94 (t, CH_2^d, 2H), 3.18 (s, CH_2^b, 2H), 3.01 (q, CH_2^j, 2H), 2.71 (t, CH_2^e, 2H), 2.37 (m, CH_2^i/CH_2^h, 4H), 2.15 (s, CH_3^{pz}, 3H), 2.14 (s, CH_3^{pz}, 3H), 2.07 (t, CH_2^g, 2H), 1.76 - 1.66 (m, CH_2^f, 2H), 1.37(s, CH_3, 9H), 1.36 (s, CH_3, 9H), 1.15 (q, OCH_2CH_3, 2H). ^{13}C NMR (75.3 MHz, $CDCl_3$) δ_C: 173.9 (CO), 171.2 (CO), 156.4 (CO), 146.6 (C^c), 137.1 (C^a), 109.9 (C^{pz}), 80.8 ($C(CH_3)$), 79.1 ($C(CH_3)$), 60.5 (CH_2), 53.9 (CH_2), 53.8 (CH_2); 53.5 (CH_2), 49.9 (CH_2), 47.5 (CH_2), 38.7 (CH_2), 31.7 (CH_2), 28.7 ($C(CH_3)$), 28.2 ($C(CH_3)$), 22.6 (CH_2), 14.5 (CH_3), 12.0 (CH_3^{pz}), 10.0 (CH_3^{pz}).

4-((2-(4-(2-tert-Butoxy-2-oxoethyl)-3,5-dimethyl-1H-pyrazol-1-yl)ethyl)(2-(tert-butoxycarbonylamino)ethyl)amino)butanoic Acid (t-BuPz^4(Boc)). A solution of **6** (0.23 g, 0.45 mmol) and excess NaOH (0.75 g, 2.10 mmol) in H_2O/THF were stirred overnight, at room temperature. After neutralization with HCl 1 M at 0 °C and solvent evaporation under reduced pressure, the residue was purified by flash chromatography (silica gel, dichloromethane/methanol, 0−20%), giving *t*-BuPz^4(Boc) as a white solid. Yield: 67% (0.14 g; 0.29 mmol). ^{1}H NMR (300 MHz, $CDCl_3$) δ_H: 4.08 (t,CH_2^d, 2H), 3.21 (s, CH_2^b, 2H), 3.04 (q, CH_2^e, 2H), 2.83 (t, CH_2^g, 2H), 2.57 (t, CH_2^f, 2H), 2.49 (t, CH_2^h, 2H), 2.36 (t, CH_2^j, 2H), 2.1 (s, CH_3^{pz}, 3H), 2.03 (s, CH_3^{pz}, 3H), 1.86 (t, CH_2^i, 2H), 1.24 (s, CH_3, 18H). ^{13}C NMR (75.3 MHz, $CDCl_3$) δ_C: 189.8 (CO), 187.6 (CO), 165.1 (CO), 154.5 (C^c), 145.9 (C^a), 119.4 (C^{pz}), 81.0 ($C(CH_3)_3$), 79.1 ($C(CH_3)_3$), 60.2 (C^h), 59.7 (C^e), 59.2 (C^f), 52.4 (C^d), 44.1 (C^g), 42.3 (C^j), 38.8 (C^b), 34.8 ($C(CH_3)$), 29.5 (C^i), 17.7 (CH_3^{pz}), 15.9 (CH_3^{pz}). RP-HPLC (220 nm, gradient A): 99% (t_R = 19.9 min). ESI-MS (+) (m/z): 483.7 [M + H]$^+$, calcd for $C_{24}H_{42}N_4O_6$ = 482.6.

Synthesis of βAlaNleCycMSH$_{hex}$. The linear sequence Fmoc-Asp(Dmab)-His(Trt)-DPhe-Arg(Pbf)-Trp(Boc)-Lys(ivDde)-NH_2 was assembled to MBHA Rink Amide resin by Fmoc-based solid phase peptide synthesis (SPPS) in a CEM 12-channel automated peptide, while βAlaNleCycMSH$_{hex}$ was obtained through the synthetic route described in the literature.[11] After cleavage from the resin and semipreparative RP-HPLC (gradient B) purification, the Fmoc-βAlaNleCycMSH$_{hex}$ was obtained as a white solid that was characterized by ESI-MS (calculated m/z for [M + H]$^+$, 1275.6; found:, 1275.6). RP-HPLC (220 nm, gradient B): 99% (t_R = 25.8 min). The protected peptide was treated with solution of 20% piperidine in DMF and after solvent evaporation the residue was washed with ice cold ether, yielding βAlaNleCycMSH$_{hex}$ as a white solid. The peptide was suspended in water, lyophilized, and characterized by ESI-MS (calculated m/z for [M + H]$^+$, 1052.6; found, 1053.6). RP-HPLC (220 nm, gradient B): 99% (t_R = 16.5 min).

Synthesis of the Peptide Conjugates. The peptide conjugates Pz^2-βAlaNleCycMSH$_{hex}$−Pz^4-βAlaNleCycMSH$_{hex}$ were prepared using the following procedure: approximately 800 μg of peptide were dissolved in *N*,*N*-diisopropylethylamine (20 μL)/dimethylformamide (250 μL) before added Pz^2(Boc), Pz^3(Boc) or *t*-Bupz^4(Boc) (2.5 equiv) preincubated for 30 min with HATU (1.1 equiv relative to each carboxylic group). After stirring for 3 h at room temperature, the reaction mixture was purified by semipreparative RP-HPLC (gradient B). The peptide conjugates were characterized by ESI-MS (Table 1) after removal of the Boc protecting group with standard cocktail (95% TFA, 2.5% TIS, 2.5% H_2O), precipitation with ice-cold diethyl ether, and lyophilization.

Structural Characterization of Peptide Conjugate. NMR samples of Pz^3 and Pz^3-βAlaNleCycMSH$_{hex}$ were prepared by dissolving the lyophilized compounds, ∼5 mg and ∼0.65 mg, respectively, in 0.5 mL of H_2O/D_2O (9:1 v/v). pH was adjusted to 2.5 by adding minimal amounts of NaOD or DCl, measured with a glass microelectrode, and not corrected for isotope effects. Sodium 2,2-dimethyl-2-silapentane-5-sulfonate (DSS) was added as an internal reference. NMR spectra of Pz^3 and Pz^3-βAlaNleCycMSH$_{hex}$ were acquired at 25 °C on a Bruker AV-600 spectrometer operating at a proton frequency of 600.13 MHz and equipped with a cryoprobe. Two-dimensional spectra, i.e., ^{1}H−^{1}H phase-sensitive correlated spectroscopy (COSY), total correlated spectroscopy (TOCSY), and rotating frame nuclear Overhauser spectroscopy (ROESY), as well as ^{1}H−^{13}C and ^{1}H−^{15}N heteronuclear single quantum coherence spectra (HSQC) at natural heteronuclear abundance, were recorded as previously reported.[29] TOCSY spectra were acquired using 60 ms DIPSI2 with *z* filter spin-lock sequence and ROESY mixing time was 200 ms. For each sample, two different ^{1}H−^{13}C-HSQC spectra were acquired, one optimized for aliphatic $^1J_{C-H}$ coupling constants and the other for $^1J_{C-H}$ of aromatic rings (pyrazole, His, Trp, and DPhe). Data were processed using the standard TOPSPIN program (Bruker Biospin. Karlsruhe, Germany). The 0 ppm ^{13}C and ^{15}N δ-values were obtained indirectly by multiplying the spectrometer frequency that corresponds to 0 ppm in the ^{1}H spectrum, assigned to internal DSS reference, by 0.25144953 and 0.101329118, respectively.[30] NMR spectra were analyzed using the Sparky program.[31]

Radiolabeling with ^{99m}Tc(I). Na[^{99m}TcO4] was eluted from a ^{99}Mo/^{99m}Tc generator, using 0.9% saline. The precursor *fac*-[^{99m}Tc-$(CO)_3(H_2O)_3]^+$ was prepared using the Isolink kit and its radiochemical purity checked by RP-HPLC.

Complexes ^{99m}Tc(CO_3)-Pz^2-βAlaNleCycMSH$_{hex}$−^{99m}Tc(CO_3)-Pz^4-βAlaNleCycMSH$_{hex}$ were obtained by reaction of peptide conjugates Pz^2-βAlaNleCycMSH$_{hex}$−Pz^4-βAlaNleCycMSH$_{hex}$ with *fac*-[^{99m}Tc-$(CO)_3(H_2O)_3]^+$, respectively. Briefly, the peptide conjugates were labeled after a solution of *fac*-[^{99m}Tc$(CO)_3(H_2O)_3]^+$ (900 μL) was added to a capped vial, previously flushed with N_2, containing Pz^2-βAlaNleCycMSH$_{hex}$−Pz^4-βAlaNleCycMSH$_{hex}$ (100 μL, 5 × 10^{-4} M). The mixture reacted for 30 min, at 90 °C, and the radiochemical purity of ^{99m}Tc(CO_3)-Pz^2-βAlaNleCycMSH$_{hex}$−^{99m}Tc(CO_3)-Pz^4-βAlaNleCycMSH$_{hex}$ was checked by RP-HPLC (gradient C), using an analytical C-18 reversed-phase column. The radiolabeled compound was purified by semipreparative RP-HPLC (gradient D). The activity corresponding to ^{99m}Tc$(CO)_3$−peptide conjugates was collected in a 50 mL Falcon flask, containing 200 μL of PBS with 0.2% BSA, and purged with N_2 gas for 20 min to remove the acetonitrile. The pH of the final solution was adjusted to 7.4 with 0.1 M NaOH for biodistribution and internalization studies. The product was controlled by analytical RP-HPLC (gradient D) to confirm its purity and stability after purification and evaporation.

Cysteine and Histidine Challenge. Aliquots of the ^{99m}Tc(CO_3)-Pz^2-βAlaNleCycMSH$_{hex}$−^{99m}Tc(CO_3)-Pz^4-βAlaNleCycMSH$_{hex}$ (100 μL) were added to 5 × 10^{-3} M cysteine or histidine solutions in PBS pH 7.4 (400 μL). The resulting solutions were incubated at 37 °C

for 24 h and analyzed by analytical RP-HPLC using the method described in the chromatographic section.

Partition Coefficient. Partition coefficient was evaluated by the "shake-flask" method.[24] The radioactive peptide conjugate was added to a mixture of octanol (1 mL) and 0.1 M PBS pH 7.4 (1 mL), previously saturated with each other by stirring. This mixture was vortexed and centrifuged (3000 rpm, 10 min) to allow phase separation. Aliquots of both octanol and PBS were counted in a γ counter. The partition coefficient ($P_{o/w}$) was calculated by dividing the counts in the octanol phase by those in the buffer.

In Vitro Stability. The in vitro stability of the radiopeptides was determined in human serum. The ^{99m}Tc-labeled complex (100 μL, ≈10 MBq) was added to human serum (1 mL), and the mixture was incubated at 37 °C. At appropriate time points (2, 4, and 6 h), 100 μL aliquots (in duplicate) were sampled and treated with 200 μL of ethanol to precipitate the proteins. Samples were centrifuged at 3000 rpm for 15 min at 4 °C, and the supernatant was analyzed by HPLC. The stability of the radiolabeled conjugate in the solutions containing 0.2% BSA was checked by RP-HPLC using the chromatographic methods previously described and by instant thin-layer chromatography-SG (5% 6 N HCl in MeOH).

Cell Culture. B16F1 murine melanoma cells (ECACC, England, UK) were grown in DMEM containing GlutaMax I supplemented with 10% heat-inactivated fetal bovine serum and 1% penicillin/streptomycin antibiotic solution (all from Gibco-Invitrogen). Cells were cultured in a humidified atmosphere of 95% air and 5% CO_2 at 37 °C (Heraeus, Germany), with the medium changed every other day. The cells were adherent in monolayers and, when confluent, were harvested from the cell culture flasks with trypsin EDTA (Gibco-Invitrogen) and seeded further apart.

[^{125}I]NDP-α-MSH. Radioiodination of NDP-α-MSH with ^{125}I was performed by the chloramine-T method.[26] Preceding each binding experiment, an additional purification was performed by RP-HPLC.[26]

Internalization and Cellular Retention Studies. Internalization assays of the radiopeptides were performed in B16F1 murine melanoma cells seeded at a density of 0.2 million per well in plates and allowed to attach overnight. The cells were incubated at 37 °C for a period of 5 min to 4 h with about 200000 cpm of the conjugate in 0.5 mL of assay medium (MEM with 25 mM *N*-(2-hydroxyethyl)-piperazine-*N*-ethanesulfonic acid and 0.2% BSA). Incubation was terminated by washing the cells with ice-cold assay medium. Cell-surface-bound radioligand was removed by two steps of acid wash (50 mM glycine, HCl/100 mM NaCl, pH 2.8) at room temperature for 5 min. The pH was neutralized with cold PBS with 0.2% BSA, and subsequently the cells were lysed by 10 min incubation with 1 M NaOH at 37 °C to determine internalized radioligand. For assessing the specific MC1R-mediated uptake and internalization at 1 and 2 h, a parallel study was performed using the potent agonist NDP-MSH (3.5 μg/well) for saturating the MC1R.

To determine the retention properties of the internalized radioconjugates, B16F1 cells were first incubated with the radioligands for 3 h at 37 °C to allow internalization. The cells were washed with cold assay medium (to stop the internalization) and with acid buffer (to remove the membrane-bound radioactivity). Finally, the cells were incubated with culture medium (0.5 mL) during 4 h at 37 °C. At different time points (10 min, 1, 2, 3, and 4 h), the radioactivity released in the medium (externalized radioactivity) as well as the radioactivity retained in the cells (lysed with NaOH, 1M) was collected and counted.

Biodistribution. All animal experiments were performed in compliance with national and European regulations for animal treatment. The animals were housed in a temperature- and humidity-controlled room with a 12 h light/12 h dark schedule. Biodistribution of the radiopeptides was performed in melanoma-bearing C57BL/6 female mice (8–10 weeks old). Mice were previously implanted subcutaneously with 1×10^6 B16F1 cells to generate a primary skin melanoma. Ten to 12 days after the inoculation, tumors reached a weight of 0.2–1 g.

Animals were intravenously injected into the retroorbital sinus with the radiolabeled complex (2.6–3.7 GBq) diluted in 100 μL of PBS pH 7.2. Mice were killed by cervical dislocation at 1 and 4 h after injection. The dose administered and the radioactivity in the killed animals was measured using a dose calibrator (Curiemeter IGC-3, Aloka, Tokyo, Japan or Carpintec CRC-15W, Ramsey, USA). The difference between the radioactivity in the injected and that in the killed animals was assumed to be due to excretion. Tumors and normal tissues of interest were dissected, rinsed to remove excess blood, and weighed, and their radioactivity was measured using a γ-counter (LB2111, Berthold, Germany). The uptake in the tumor and healthy tissues of interest was calculated and expressed as a percentage of the injected radioactivity dose per gram of tissue. For blood, bone, muscle, and skin, total activity was estimated assuming that these organs constitute 6, 10, 40, and 15% of the total body weight, respectively. Urine was also collected and pooled together at the time the animals were killed, filtered through a Millipore filter (0.22 μm), and also analyzed by RP-HPLC. The specificity of tumor uptake for ^{99m}Tc(CO$_3$)-Pz^3-βAlaNleCycMSH$_{hex}$ and ^{99m}Tc(CO$_3$)-Pz^4-βAlaNleCycMSH$_{hex}$ was determined by coinjecting 20 μg (12.1 nmol) of unlabeled NDP-MSH, which is a well-known linear α-MSH analogue with picomolar MC1R binding affinity.

In Vivo Stability. The stability of the complexes was assessed by RP-HPLC analysis of urine and serum, under identical conditions to those used for analyzing the original radiopeptides. Tissue (kidney, liver, and tumor) homogenates were used to further assess the stability of radiopeptides in the presence of cellular enzymes. The samples were taken 1 and 4 h after injection. The urine collected at the time the mice were killed was filtered through a Millex GV filter (0.22 μm) before analysis. Blood collected from the mice was centrifuged at 3000 rpm for 15 min at 4 °C, and the serum was separated. The serum was treated with ethanol in a 2:1 (v/v) ratio to precipitate the proteins. After centrifugation at 3000 rpm for 15 min at 4 °C, the supernatant was collected and analyzed by RP-HPLC. Liver, kidney, and tumor were homogenized with a glass-homogenizer (Potter) in 50 mM Tris buffer with 0.2 M sucrose, pH 7.4. The homogenate was then centrifuged at 4 °C (20000*g* for 10 min). The supernatant was treated with ethanol in a 1:1 (v/v) ratio to precipitate the proteins, centrifuged again, and the resulting supernatant injected into the HPLC.

■ ASSOCIATED CONTENT

Supporting Information

ESI-MS spectral data of the peptide conjugates, NMR characterization of Pz^3 and Pz^3-βAlaNleCycMSH$_{hex}$, RP-HPLC chromatogram of ^{99m}Tc-Pz^4-βAlaNleCycMSH$_{hex}$ purification, RP-HPLC chromatograms of tumor, kidney, and liver homogenate at 1 h and 4 h pi of Pz^3-βAlaNleCycMSH$_{hex}$. This material is available free of charge via the Internet at http://pubs.acs.org.

■ AUTHOR INFORMATION

Corresponding Author

*Phone: +351219946201. Fax: 351 21 994 6185. E-mail: isantos@itn.pt.

Notes

The authors declare no competing financial interest.

■ ACKNOWLEDGMENTS

M. Morais and B. L. Oliveira thanks the Fundação para a Ciência e Tecnologia for Ph.D. fellowships (SFRH/BD/48066/2008 and SFRH/BD/38753/2007, respectively), Covidean-Mallinckrodt for the kits, and Dr. J. Marçalo for performing the ESI-MS analyses. The ESI/QITMS was acquired with the support of the Programa Nacional de Reequipamento Científico of FCT and is part of RNEM-Rede Nacional de Espectrometria de Massa also supported by FCT. M. A. Jiménez thanks the financial support from Spanish MICINN project CTQ2011-22514. Dr. G. Cantinho and Rafael Pinto are

acknowledged for the gamma camera imaging studies with melanoma-bearing C57BL/6 female mice.

■ ABBREVIATIONS USED

α-MSH, Ac-Ser-Tyr-Ser-Met-Glu-His-Phe-Arg-Trp-Gly-Lys-Pro-Val-NH_2; DOTA, 1,4,7,10-tetraazacyclododecane-1,4,7,10-tetraacetic acid; NOTA, triazacyclononane-1,4,7-triacetic acid; SPECT, single-photon emission computed tomography; % IA/g, percentage injected activity per gram; pi, post injection; BFC, bifunctional chelator; Boc, *tert*-butyloxycarbonyl; *t*-Bu, *tert*-butyl; RP-HPLC, reverse-phase high performance liquid chromatography; ESI-MS, ionization−mass spectrometry; HATU, 2-(7-aza-1*H*-benzotriazole-1-yl)-1,1,3,3-tetramethyluronium hexafluorophosphate; DIPEA, diisopropylethylamine; TIS, triisopropylsilane; ROE, rotating frame Overhauser effect; NDP-α-MSH, Ac-Ser-Tyr-Ser-Nle-Glu-His-DPhe-Arg-Trp-Gly-Lys-Pro-Val-NH_2; DMEM, Dulbecco'S Modified Eagle'S Medium; SPPS, solid-phase peptide synthesis; Fmoc, fluorenylmethoxycarbonyl; $P_{o/w}$, partition coefficient

■ REFERENCES

(1) Correia, J. D.; Paulo, A.; Raposinho, P. D.; Santos, I. Radiometallated peptides for molecular imaging and targeted therapy. *J. Chem. Soc., Dalton Trans.* **2011**, *40*, 6144−6167.

(2) Reubi, J. C.; Maecke, H. R. Peptide-based probes for cancer imaging. *J. Nucl. Med.* **2008**, *49*, 1735−1738.

(3) Lee, S.; Xie, J.; Chen, X. Peptide-based probes for targeted molecular imaging. *Biochemistry* **2010**, *49*, 1364−1376.

(4) Raposinho, P. D.; Correia, J. D. G.; Oliveira, M. C.; Santos, I. Melanocortin-1 Receptor-Targeting With Radiolabeled Cyclic alpha-Melanocyte-Stimulating Hormone Analogs for Melanoma Imaging. *Biopolymers* **2010**, *94*, 820−829.

(5) Wei, L.; Zhang, X.; Gallazzi, F.; Miao, Y.; Jin, X.; Brechbiel, M. W.; Xu, H.; Clifford, T.; Welch, M. J.; Lewis, J. S.; Quinn, T. P. Melanoma imaging using (111)In-, (86)Y- and (68)Ga-labeled CHX-A″-Re(Arg11)CCMSH. *Nucl. Med. Biol.* **2009**, *36*, 345−354.

(6) Miao, Y. B.; Benwell, K.; Quinn, T. P. (99)mTc and In-111-labeled alpha-melanocyte-stimulating hormone peptides as imaging probes for primary and pulmonary metastatic melanoma detection. *J. Nucl. Med.* **2007**, *48*, 73−80.

(7) Guo, H.; Yang, J.; Gallazzi, F.; Miao, Y. Reduction of the ring size of radiolabeled lactam bridge-cyclized alpha-MSH peptide, resulting in enhanced melanoma uptake. *J. Nucl. Med.* **2010**, *51*, 418−426.

(8) Guo, H. X.; Yang, J. Q.; Gallazzi, F.; Miao, Y. B. Effects of the Amino Acid Linkers on the Melanoma-Targeting and Pharmacokinetic Properties of (111)In-Labeled Lactam Bridge-Cyclized alpha-MSH Peptides. *J. Nucl. Med.* **2011**, *52*, 608−616.

(9) Guo, H.; Yang, J.; Shenoy, N.; Miao, Y. Gallium-67-labeled lactam bridge-cyclized alpha-melanocyte stimulating hormone peptide for primary and metastatic melanoma imaging. *Bioconjugate Chem.* **2009**, *20*, 2356−2363.

(10) Guo, H. X.; Gallazzi, F.; Miao, Y. B. Gallium-67-Labeled Lactam Bridge-Cyclized Alpha-MSH Peptides with Enhanced Melanoma Uptake and Reduced Renal Uptake. *Bioconjugate Chem.* **2012**, *23*, 1341−1348.

(11) Valldosera, M.; Monso, M.; Xavier, C.; Raposinho, P.; Correia, J. D. G.; Santos, I.; Gomes, P. Comparative study of chemical approaches to the solid-phase synthesis of a tumor-seeking alpha-MSH analogue. *Int. J. Pept. Res. Ther.* **2008**, *14*, 273−281.

(12) Raposinho, P. D.; Xavier, C.; Correia, J. D. G.; Falcao, S.; Gomes, P.; Santos, I. Melanoma targeting with alpha-melanocyte stimulating hormone analogs labeled with fac-[Tc-99m(CO)(3)](+): effect of cyclization on tumor-seeking properties. *J. Biol. Inorg. Chem.* **2008**, *13*, 449−459.

(13) Decristoforo, C.; Mather, S. J. The influence of chelator on the pharmacokinetics of 99mTc-labelled peptides. *Q. J. Nucl. Med.* **2002**, *46*, 195−205.

(14) Mather, S. J. Design of radiolabelled ligands for the imaging and treatment of cancer. *Mol. Biosyst.* **2007**, *3*, 30−35.

(15) Froidevaux, S.; Calame-Christe, M.; Tanner, H.; Eberle, A. N. Melanoma targeting with DOTA-alpha-melanocyte-stimulating hormone analogs: structural parameters affecting tumor uptake and kidney uptake. *J. Nucl. Med.* **2005**, *46*, 887−895.

(16) Akizawa, H.; Arano, Y.; Mifune, M.; Iwado, A.; Saito, Y.; Mukai, T.; Uehara, T.; Ono, M.; Fujioka, Y.; Ogawa, K.; Kiso, Y.; Saji, H. Effect of molecular charges on renal uptake of In-111-DTPA-conjugated peptides. *Nucl. Med. Biol.* **2001**, *28*, 761−768.

(17) Bapst, J. P.; Calame, M.; Tanner, H.; Eberle, A. N. Glycosylated DOTA-alpha-Melanocyte-Stimulating Hormone Analogues for Melanoma Targeting: Influence of the Site of Glycosylation on in Vivo Biodistribution. *Bioconjugate Chem.* **2009**, *20*, 984−993.

(18) Froidevaux, S.; Calame-Christe, M.; Tanner, H.; Sumanovski, L.; Eberle, A. N. A novel DOTA-alpha-melanocyte-stimulating hormone analog for metastatic melanoma diagnosis. *J. Nucl. Med.* **2002**, *43*, 1699−1706.

(19) Palma, E.; Oliveira, B. L.; Correia, J. D. G.; Gano, L.; Maria, L.; Santos, I. C.; Santos, I. A new bisphosphonate-containing Tc-99m(I) tricarbonyl complex potentially useful as bone-seeking agent: synthesis and biological evaluation. *J. Biol. Inorg. Chem.* **2007**, *12*, 667−679.

(20) Oliveira, B. L.; Raposinho, P. D.; Mendes, F.; Santos, I. C.; Santos, I.; Ferreira, A.; Cordeiro, C.; Freire, A. P.; Correia, J. D. G. Targeting nitric oxide synthase with (99m)Tc/Re-tricarbonyl complexes containing pendant guanidino or isothiourea moieties. *J. Organomet. Chem.* **2011**, *696*, 1057−1065.

(21) Esteves, T.; Marques, F.; Paulo, A.; Rino, J.; Nanda, P.; Smith, C. J.; Santos, I. Nuclear targeting with cell-specific multifunctional tricarbonyl M(I) (M is Re, Tc-99m) complexes: synthesis, characterization, and cell studies. *J. Biol. Inorg. Chem.* **2011**, *16*, 1141−1153.

(22) Morais, M.; Subramanian, S.; Pandey, U.; Samuel, G.; Venkatesh, M.; Martins, M.; Pereira, S.; Correia, J. D.; Santos, I. Mannosylated dextran derivatives labeled with fac-[M(CO)] + (M = (99m)Tc, Re) for specific targeting of sentinel lymph node. *Mol. Pharmaceutics* **2011**, *8*, 609−620.

(23) Alves, S.; Paulo, A.; Correia, J. D. G.; Gano, L.; Smith, C. J.; Hoffman, T. J.; Santos, I. Pyrazolyl derivatives as bifunctional chelators for labeling tumor-seeking peptides with the fac-[M(CO)(3)](+) moiety (M = Tc-99m, Re): synthesis, characterization, and biological behavior. *Bioconjugate Chem.* **2005**, *16*, 438−449.

(24) Troutner, D. E.; Volkert, W. A.; Hoffman, T. J.; Holmes, R. A. A Neutral Lipophilic Complex of Tc-99m with a Multidentate Amine Oxime. *Int. J. Appl. Radiat. Isot.* **1984**, *35*, 467−470.

(25) Raposinho, P. D.; Correia, J. D. G.; Alves, S.; Botelho, M. F.; Santos, A. C.; Santos, I. A Tc-99m(CO)(3)-labeled pyrazolyl-alpha-melanocyte-stimulating hormone analog conjugate for melanoma targeting. *Nucl. Med. Biol.* **2008**, *35*, 91−99.

(26) Morais, M.; Raposinho, P. D.; Oliveira, M. C.; Correia, J. D. G.; Santos, I. Evaluation of novel Tc-99m(I)-labeled homobivalent alpha-melanocyte-stimulating hormone analogs for melanocortin-1 receptor targeting. *J. Biol. Inorg. Chem.* **2012**, *17*, 491−505.

(27) Morais, M.; Raposinho, P. D.; Oliveira, M. C.; Pantoja-Uceda, D.; Jimenez, M. A.; Santos, I.; Correia, J. D. G. NMR Structural Analysis of MC1R-Targeted Rhenium(I) Metallopeptides and Biological Evaluation of Tc-99m(I) Congeners. *Organometallics* **2012**, *31*, 5929−5939.

(28) Guo, H.; Yang, J.; Gallazzi, F.; Prossnitz, E. R.; Sklar, L. A.; Miao, Y. Effect of DOTA Position on Melanoma Targeting and Pharmacokinetic Properties of 111In-labeled Lactam Bridge-Cyclized Alpha-Melanocyte Stimulating Hormone Peptide. *Bioconjugate Chem.* **2009**, *20*, 2162−2168.

(29) Mirassou, Y.; Santiveri, C. M.; de Vega, M. J. P.; Gonzalez-Muniz, R.; Jimenez, M. A. Disulfide Bonds versus Trp center dot center dot center dot Trp Pairs in Irregular beta-Hairpins: NMR Structure of Vammin Loop 3-Derived Peptides as a Case Study. *ChemBioChem* **2009**, *10*, 902−910.

(30) Wishart, D. S.; Bigam, C. G.; Yao, J.; Abildgaard, F.; Dyson, H. J.; Oldfield, E.; Markley, J. L.; Sykes, B. D. 1H, 13C and 15N chemical

shift referencing in biomolecular NMR. *J. Biomol. NMR* **1995**, *6*, 135−140.
(31) Goddard, T. D.; Kneller, D. G. *SPARKY 3*; University of California: San Francisco, 1999.